Acta Crystallographica Section D
Biological Crystallography
ISSN 0907-4449

Actin–DBP: the perfect structural fit?

Christel Verboven,[a] Ilse Bogaerts,[a] Etienne Waelkens,[b] Anja Rabijns,[a] Hugo Van Baelen,[c] Roger Bouillon[c] and Camiel De Ranter[a]*

[a]Laboratorium voor Analytische Chemie en Medicinale Fysicochemie, Faculteit Farmaceutische Wetenschappen, K. U. Leuven, Belgium, [b]Afdeling Biochemie, Onderwijs en Navorsing, K. U. Leuven, Belgium, and [c]Laboratorium voor Experimentele Geneeskunde en Endocrinologie, K. U. Leuven, Belgium

Correspondence e-mail: camiel.deranter@pharm.kuleuven.ac.be

Received 8 July 2002
Accepted 20 November 2002

PDB Reference: actin–DBP, 1ma9, r1ma9sf.

The multifunctional vitamin D binding protein (DBP) is an actin-sequestering protein present in blood. The crystal structure of the actin–DBP complex was determined at 2.4 Å resolution. DBP binds to actin subdomains 1 and 3 and occludes the cleft at the interface between these subdomains. Most remarkably, DBP demonstrates an unusually large actin-binding interface, far exceeding the binding-interface areas reported for other actin-binding proteins such as profilin, DNase I and gelsolin. The fast-growing side of actin monomers is blocked completely through a perfect structural fit with DBP, demonstrating how DBP effectively interferes with actin-filament formation. It establishes DBP as the hitherto best actin-sequestering protein and highlights its key role in suppressing and preventing extracellular actin polymerization.

1. Introduction

Actin is a highly abundant intracellular protein present in all eukaryotic cells and has a pivotal role in muscle contraction as well as in cell movements. Actin also has an essential function in maintaining and controlling cell shape and architecture: it is the essential building block of the microfilament system, a cytoskeletal structure which complements two other cytoskeletal structures (the microtubules and the intermediate filaments). In low-salt buffers, actin exists as a monomeric protein (globular actin; G-actin), but it polymerizes under physiological salt conditions into a double-helical 10 nm thick filament structure (filamentous actin; F-actin). *In vivo*, the equilibrium between G-actin and F-actin is controlled mainly by the action of several actin-binding proteins with distinct activities (*e.g.* gelsolin, profilin, *etc.*).

In conditions involving severe cell injury, such as trauma, shock, sepsis and fulminant hepatic necrosis, large quantities of actin are released in the systemic circulation. The presence of actin filaments in blood, leading to an increase in blood viscosity, is dangerous and can be fatal (Lee & Galbraith, 1992). In addition, actin can promote clot formation by its ability to aggregate platelets (Vasconcellos & Lind, 1993). Therefore, the presence of a protective system preventing actin polymerization and ensuring actin's fast elimination is essential.

The vitamin D binding protein (DBP), a plasma protein which is also known as group-specific component or Gc-globulin, is an actin-binding protein (Van Baelen *et al.*, 1980; White & Cooke, 2000) and acts as an actin-sequestering agent in extracellular space. DBP and gelsolin, the only other plasma protein that binds actin avidly, play a crucial role in the clearance of actin filaments from the circulation, a process known as the 'actin-scavenger system' (Lee & Galbraith,

Table 1
Statistics of the crystallographic analysis.

Values in parentheses pertain to the highest resolution shell.

Data collection	
Space group	$P2_1$
Unit-cell parameters (Å, °)	a = 74.4, b = 74.9, c = 88.0, β = 110.2
Wavelength (Å)	0.8423
Resolution range (Å)	20–2.40 (2.44–2.40)
Observations/unique reflections	97747/33252
Completeness (%)	93.3 (93.9)
$\langle I/\sigma(I)\rangle$†	12.2 (1.8)
R_{sym}‡ (%)	4.2 (25.0)
Refinement	
Reflections (working/test)	29736/2455
Non-H atoms	
Protein	6157
ATP	31
Water atoms	289
Magnesium ions	1
R_{cryst}§ (%)	19.83
R_{free}§ (%)	25.32
R.m.s.d. bond lengths (Å)	0.006
R.m.s.d. bond angles (°)	1.162
R.m.s.d. B, bonded main chain (Å^2)	1.387
R.m.s.d. B, bonded side chain (Å^2)	2.055

† $\langle I/\sigma(I)\rangle$ is the mean signal-to-noise ratio, where I is the integrated intensity of a measured reflection and $\sigma(I)$ is the estimated error in the measurement. ‡ $R_{sym} = \sum_h \sum_i |I_{h,i} - \langle I_h\rangle| / \sum_h \sum_i I_{h,i}$, where I is the integrated intensity of reflection h having i observations. § $R_{cryst} = \sum |F_{obs} - F_{calc}| / \sum F_{obs}$, where F_{obs} and F_{calc} are the observed and calculated structure-factor amplitudes. R_{free} is calculated similarly using test-set reflections, which are randomly chosen and never used during refinement.

1992). Gelsolin has three actin-binding properties: (i) it severs F-actin, (ii) it caps the end of F-actin and (iii) it nucleates actin-filament assemblies. Gelsolin will shift the equilibrium between actin assembly/disassembly towards actin depolymerization, but will not basically prevent actin reassembly. By forming a complex with G-actin, DBP prevents the (re-)formation of actin filaments. Therefore, DBP and gelsolin have complementary functions: upon severing of the actin filaments by gelsolin, the generated globular actin is locked in its monomeric state by DBP. Clearance of this actin–DBP complex is substantially faster than clearance of free DBP (Lind *et al.*, 1986; Goldschmidt-Clermont *et al.*, 1988; Dueland *et al.*, 1991; Herrmannsdoerfer *et al.*, 1993). The complementary action of both proteins is further illustrated by the previous observation that both DBP and gelsolin are required to inhibit actin-stimulated platelet aggregation (Vasconcellos & Lind, 1993).

The severing and capping activities of gelsolin have been investigated extensively by structural studies of plasma gelsolin itself (Burtnick *et al.*, 1997) and of various gelsolin segments in complex with actin (McLaughlin *et al.*, 1993; Robinson *et al.*, 1999). Until very recently, no structural data were available for the role of DBP in the actin-scavenger system (Otterbein *et al.*, 2002; Head *et al.*, 2002). Here, we report the crystal structure of actin in complex with DBP. This paper provides evidence for the pronounced role of DBP in preventing actin polymerization in the circulation. This study even indicates that some regions in the F-actin model must be folded differently in order to fit our observations. This paper also provides some answers to other questions related to the various functions of DBP in the circulation. (i) Given the high DBP plasma concentration (4–8 μM) compared with the circulating concentrations of vitamin D and its metabolites, less than 5% of the circulating DBP is complexed with vitamin D compounds (Cooke & Haddad, 1989). Although the purpose of this large excess is believed to be related to the other functions of DBP, *i.e.* its roles in the extracellular actin-scavenger system, in the immune system and in free fatty-acid transport, the primary function of DBP in the circulation is still not fully elucidated. (ii) The actin–DBP structure also illustrates how actin and vitamin D can simultaneously bind to DBP. (iii) It also provides a structural explanation for the reason why DBP binds actin while the structurally related human serum albumin (HSA), α-fetoprotein and afamin do not interact with actin.

2. Materials and methods

2.1. Structure determination of the actin–DBP complex

Crystals of rabbit muscle actin (375 amino acids) in complex with human DBP (458 amino acids) and adenosine 5′-triphosphate (ATP) were obtained as described previously (Bogaerts *et al.*, 2001). These crystals belong to the monoclinic space group $P2_1$. A data set to 2.3 Å was collected at 100 K on beamline BW7B at the DESY synchrotron facility (Germany). These data were processed using the *HKL* package (Otwinowski & Minor, 1997). Initial phase information was obtained by molecular replacement using the routines present in the *CNS* package (Brünger *et al.*, 1998) and the known structures of actin (PDB code 1atn; Kabsch *et al.*, 1990) and DBP (PDB code 1j78; Verboven *et al.*, 2002) as search probes. The program *O* (Jones *et al.*, 1991) was used for model building. The actin–DBP structure was refined with *CNS* (Brünger *et al.*, 1998) using torsion-angle dynamics and restrained individual *B*-factor refinement. During refinement, solvent molecules were progressively added when they met the following criteria: (i) a minimum 3σ peak was present in the $|F_{obs}| - |F_{calc}|$ difference map, (ii) a peak was visible in the $2|F_{obs}| - |F_{calc}|$ map, (iii) the B value for the water molecule did not exceed 80 Å^2 during refinement and (iv) the water molecule was stabilized by hydrogen bonding. The refinement statistics and the quality of the final model are summarized in Table 1. The actin–DBP structure has 90.3% of all its residues in the core region of the Ramachandran plot and has no residues in disallowed regions. The mean temperature factor for all atoms in the DBP structure is 55.8 Å^2, while that for all actin atoms is 48.4 Å^2 and that for the water molecules is 48.9 Å^2. The Wilson temperature factor for the data is 39.9 Å^2.

All buried surface areas were calculated with a routine present in *CNS* (Brünger *et al.*, 1998). The superposition of the structures was performed with *LSQMAN* (Kleywegt *et al.*, 2001). In all cases, only C$^\alpha$ atoms were explicitly superimposed and no additional improvement of the fit was performed. Molecular graphics were generated using *MOLSCRIPT* (Kraulis, 1991), *Raster3D* (Merritt & Murphy, 1994) and *BOBSCRIPT* (Esnouf, 1997).

2.2. Actin–DBP binding experiments

The binding of DBP to polymeric F-actin was studied using three different strategies. (i) Free DBP (at concentrations up to 0.5 mg ml^{-1}; prepared as described in Verboven *et al.*, 1995) was preincubated with 2 mg ml^{-1} G-actin (rabbit skeletal actin obtained from Sigma) in G-buffer (2 m*M* Tris–HCl pH 7.4, 0.5 m*M* 2-mercaptoethanol, 0.2 m*M* ATP) for 15–45 min at 303 K. This condition generated, besides free actin, a 1:1 DBP–actin complex, as could be demonstrated by gel filtration on Superdex 200 (data not shown). Subsequently, actin polymerization was induced by the addition of KCl to a final concentration of 150 m*M*. The insoluble polymeric F-actin was separated from the soluble proteins, including G-actin, free DBP and the 1:1 actin–DBP complex, by centrifugation for 10 min at 10 000*g*. The protein concentration in the pellet was correlated inversely with the DBP concentration, suggesting that further elongation of the actin molecule was prevented upon its association with DBP. In addition, SDS–PAGE of the pellet dissolved in SDS gel sample buffer (Laemmli, 1970), using 12% mini slab gels and Coomassie brilliant blue for staining, did not reveal the presence of DBP. (ii) DBP (at concentrations up to 0.5 mg ml^{-1}) was preincubated for 0–10 min at room temperature (RT) with actin (4 mg ml^{-1}) previously converted to its polymeric state. Protein-concentration determination in the supernatant and in pellet fractions followed the centrifugation step. Protein concentrations were determined using the bicinchoninic acid (BCA) method (Pierce, Rockford, IL, USA) with bovine serum albumin as a standard. Under these conditions, preincubation with increased DBP concentrations resulted in an equal increase of the protein concentration in the supernatant, whereas the protein concentration in the pellet did not alter significantly. This supported the idea that DBP did not coprecipitate with the actin filaments. (iii) Actin (2 mg ml^{-1}) and DBP (0.5 mg ml^{-1}) were preincubated at room temperature for 15 min. Following addition of KCl to a final concentration of 150 m*M*, a further preincubation at room temperature was performed for 15 min. The sample (200 µl) was then subjected to gel-filtration chromatography performed on a custom-made Superdex 200 HR 16/50 FPLC column (code 90-1000-90; Amersham Pharmacia Biotech) , in G-buffer supplemented with 150 m*M* KCl. The flow rate was 1 ml min^{-1}. The elution positions of proteins were determined by monitoring the absorbance at 280 nm. 0.5 ml fractions were collected. The column fractions corresponding to the elution position of molecules with a molecular weight higher than 90 kDa (∼55 kDa DBP + 43 kDa actin) were concentrated by evaporation in a Savant Speed Vac Concentrator and analyzed by SDS–PAGE. No DBP could be detected in these fractions. The purity of all protein preparations was confirmed by analysis on a Perkin Elmer SCIEX API-3000 triple-quadrupole mass spectrometer.

3. Results and discussion

3.1. General features of the actin–DBP structure

The final model of the actin–DBP structure converged to an *R* factor of 19.83% and an $R_{\rm free}$ value of 25.32%. It contains an actin, a DBP and an ATP molecule, one magnesium ion and 289 water molecules (Table 1). The all-α-helical DBP structure comprises three similar domains. Domain I (residues 1–191)

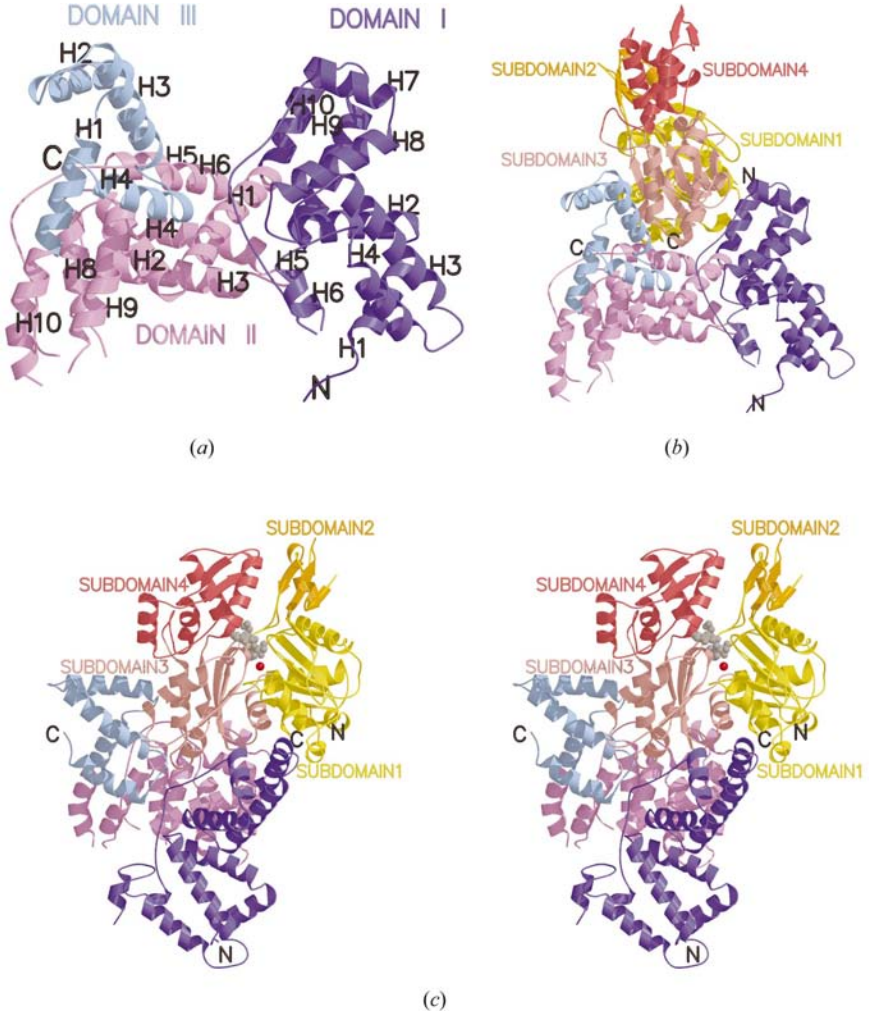

Figure 1
The structure of the actin–DBP complex. (*a*) The structure of DBP alone, illustrating its rather peculiar shape and the presence of two large grooves. The three domains of DBP are shown in different colours. The helix numbering is the same as in the uncomplexed DBP structure (Verboven *et al.*, 2002). (*b*) In the actin–DBP complex, actin binds in one of the large grooves present in the DBP structure. The four subdomains of actin are shown in different colours. (*c*) Stereo representation of the actin–DBP structure in a different orientation compared with (*b*); the molecule is rotated approximately 90° about its vertical axis. The ATP molecule bound to actin is shown as grey balls and sticks and the bound magnesium ion is shown as a red ball.

Table 2
Intermolecular contacts between actin and DBP residues.

(*a*) α-Actin.

α-Actin		DBP		
Residue	Atom	Residue	Atom	Distance (Å)
Lys113	NZ	Ser278	OG	3.51
Lys113	NZ	Asp282	OD2	3.49
Tyr143	CG	Leu184	CD1	3.64
Tyr143	OH	Leu188	CD2	3.87
Ala144	O	Thr180	CG2	3.21
Ser145	O	Asn125	OD1	3.45
Ser145	C	Thr180	CG2	3.87
Gly146	O	Asn125	OD1	3.14
Gly146	CA	Thr180	O	3.65
Gly146	O	Phe183	CB	3.57
Gly146	O	Arg187	NE	3.25
Arg147	NH2	Glu122	O	3.59
Arg147	NH1	Pro123	O	2.92
Arg147	NH1	Thr124	C	3.64
Arg147	NH1	Asn125	ND2	2.84
Arg147	NH1	Ile128	CD1	3.80
Arg147	NH1	Arg187	NH2	3.23
Thr148	CG2	Arg187	CB	3.93
Thr148	CG2	Leu188	CD2	3.85
Tyr166	CE2	Leu195	CD1	4.07
Tyr166	OH	Thr198	CG2	3.25
Tyr166	CD2	Val294	CG2	4.07
Tyr166	CD2	Phe298	CE2	3.72
Glu167	O	Lys191	NZ	2.45
Glu167	OE1	Ser194	OG	2.63
Glu167	CG	Leu195	CD1	3.34
Tyr169	CE1	Glu286	OE1	3.85
Tyr169	OH	Cys295	SG	3.28
Leu171	CD1	Phe298	CD2	3.81
His173	NE2	Phe298	O	4.02
His173	CD2	Pro300	CG	3.32
Met176	SD	Thr398	CG2	4.05†
Glu276	CG	Thr400	CG2	4.20
Tyr279	OH	Phe399	CE2	3.67‡
Tyr279	CD2	Thr400	CG2	4.01†
Asn280	OD1	Thr398	CB	3.19
Asn280	ND2	Phe399	N	3.51
Asn280	OD1	Thr400	OG1	3.00
Met283	O	Tyr394	OH	3.61
Met283	CB	Phe399	CB	3.89
Met283	CE	Ser434	CB	3.45
Lys284	NZ	Ser395	O	3.76
Lys284	NZ	Asn397	O	3.30
Asp286	OD1	Tyr297	CE2	3.74
Asp286	OD1	Asn440	CG	3.60
Asp286	OD1	Asn440	ND2	2.97
Ile287	CD1	Phe117	CE1	3.19†
Ile287	CG2	Ser434	O	3.48‡
Ile287	CG2	Asn435	OD1	3.79‡
Ile287	CD1	Pro442	CD	3.26†
Asp288	OD2	Arg202	NE	3.26
Ile289	CD1	Phe298	CZ	4.03
Arg290	NH2	Tyr394	OH	4.07
Arg290	NH2	Ser434	O	2.87
Lys291	CD	Pro118	O	3.36
Lys291	NZ	Tyr120	O	2.79
Lys291	NZ	Tyr151	OH	2.83
Ala295	CB	Val121	CG1	3.58
Lys328	NZ	Pro123	CA	3.94
Lys328	NZ	Glu127	OE1	3.19
Ile345	CG2	Leu 184	CD2	3.70
Leu346	CD1	Leu188	CD1	4.06
Leu349	CD1	Leu184	CG	4.06
Leu349	CD1	Lys185	CA	4.13
Leu349	CD1	Leu188	CD1	3.99
Thr351	OG1	Lys185	CG	4.19
Thr351	CG2	Gln189	CD	3.74
Met355	CE	Lys287	CE	4.20
His371	CB	Gln285	OE1	2.89

Table 2 (continued)

(*b*) β- or γ-Actin.

β- or γ-Actin		DBP		
Residue	Atom	Residue	Atom	Distance (Å)
Cys272	SG	Thr400	OG1	3.36†
Phe279	CE2	Phe399	CD2	3.55
Val287	CG1	Ser434	O	3.40
Val287	CG1	Asn435	OD1	3.66

† These interactions are absent in DBP–β-actin or DBP–γ-actin complexes. ‡ These residues are mutated in β- or γ-actin and have different interactions with neighbouring DBP residues. Their interactions are shown in (*b*). † This interaction is not present in DBP–α-actin.

consists of ten helices, domain II (residues 192–378) of nine helices and domain III (residues 379–458) of four helices (Verboven *et al.*, 2002). The three domains of DBP do not pack in a spherical manner, but adopt a rather peculiar shape with two large grooves (Fig. 1*a*). The structure of the actin–DBP complex reveals that G-actin binds in one of the DBP grooves, mainly formed by helix 10 of domain I, helix 6 of domain II and helix 3 of domain III, allowing DBP and actin to fit as two pieces of a jigsaw puzzle (Figs. 1*b* and 1*c*). The surface area buried at the interface of this complex is as large as 3600 Å^2. Numerous intermolecular hydrogen bonds, hydrophobic contacts and electrostatic interactions (Table 2) stabilize the complex.

The actin monomer consists of two domains, with each domain further subdivided into two subdomains (Figs. 1*b* and 1*c*). Subdomain 1 consists of residues 1–32, 70–137 and 338–375, subdomain 2 of residues 33–69, subdomain 3 of residues 138–180 and 270–337, and subdomain 4 of residues 181–269. Biochemical experiments delimited the DBP interface as residues 360–372 of actin subdomain 1 (Houmeida *et al.*, 1992). Our actin–DBP structure demonstrates that actin residues of subdomains 1 and 3 constitute the DBP-binding interface (Figs. 1*b* and 1*c*; Table 2). As in actin–gelsolin segment 1 (actin–GS1; McLaughlin *et al.*, 1993) and in actin–gelsolin segment 4–6 (actin–GS4-6; Robinson *et al.*, 1999), the binding of DBP occurs at the actin cleft formed at the interface of subdomains 1 and 3 (Fig. 1*c*). The exposed hydrophobic residues on helix 341–349 of actin subdomain 1 are thereby occluded from solvent. Even more striking is that in all these complexes the apolar patch (actin residues 341–349) is masked by a solvent-exposed hydrophobic face of a helix present in gelsolin segment 1, in gelsolin segment 4 and in DBP.

Upon complexation with DBP, the changes in the actin structure are restricted to some small regions rather than affecting the general fold. This is reflected in the small root-mean-square (r.m.s.) differences obtained from the superposition of the actin–DBP structure with actin–GS1

Table 3
Root-mean-square difference values from the superposition of our actin–DBP structure with other actin complexes.

All the values shown in the table are root-mean-square differences obtained from the superposition of the C^{α} atoms of the respective actin structure with the actin structure of the actin–DBP complex.

Superimposed part	Actin–DNase I† (Å)	Actin–gelsolin segment 1‡ (Å)	Uncomplexed actin§ (Å)
Complete structure	0.9	0.7	1.2
Subdomain 1	0.7	0.5	0.8
Subdomain 2	0.9	0.9	1.1
Subdomain 3	0.4	0.5	0.4
Subdomain 4	1.2	0.3	1.0

† The actin structure of actin–DNase I (Kabsch *et al.*, 1990) was used for the superposition. ‡ The actin structure of actin–GS1 (McLaughlin *et al.*, 1993) was used for the superposition. § The actin structure of the uncomplexed actin (Otterbein *et al.*, 2001) was used for the superposition.

(McLaughlin *et al.*, 1993), actin–DNase I (Kabsch *et al.*, 1990) and uncomplexed actin (Otterbein *et al.*, 2001) (Table 3). Similar to other actin-complex structures (McLaughlin *et al.*, 1993; Robinson *et al.*, 1999), the structural differences are mainly caused by folding changes in subdomains 2 and 4, whereas, despite their interaction with DBP, the backbone fold of subdomains 1 and 3 is hardly altered. Only the side chains of the residues at the interface adopt different orientations to ensure favourable contacts with the neighbouring DBP residues. The ATP molecule, bound in the cleft between the subdomains 2 and 4, and nearly all of the ATP surrounding residues in actin–DBP have the same orientation and conformation as found for all other known ATP–actin structures. However, the peptide bond between Glu72 and His73 is flipped, allowing a hydrogen bond between the main-chain carbonyl group of Glu72 and the side-chain atom NH1 of Arg183 (Fig. 2). The same hydrogen bond is observed in the structure of uncomplexed actin in its adenosine 5′-diphosphate (ADP) state (Otterbein *et al.*, 2001). As this hydrogen bond had never previously been observed in an ATP–actin structure, it was previously incorrectly ascribed to the presence of ADP instead of ATP and thought to form the basis for the different orientation of subdomain 4 in the ADP–actin structure (Otterbein *et al.*, 2001). Subdomain 4 does not have a different orientation in our ATP–actin structure compared with the ADP–actin structure. The r.m.s. difference between C^{α} atoms of both subdomains 4 (Table 3) is mainly caused by the different folding of residues 230–237.

Although DBP interacts with the C-terminal part of actin, located in subdomain 1, the C-terminal actin residues 372–375 are disordered in actin–DBP and show no electron density. Similar to actin–GS1 (McLaughlin *et al.*, 1993) and actin–GS4-6 (Robinson *et al.*, 1999), residues 41–50 (*i.e.* the loop that forms a β-sheet with DNase I in the actin–DNase I structure; Kabsch *et al.*, 1990) are also disordered in our structure.

According to limited proteolysis experiments performed with DBP (Haddad *et al.*, 1992), the actin-binding site is located in its C-terminal part; more specifically, residues 350–403 (of domains II and III) are involved in actin binding. However, our actin–DBP structure shows that all three DBP domains interact with actin (Figs. 1*b* and 1*c*; Table 2). Besides residues 394–395 and 397–400, both of which are parts of the biochemically identified actin-binding region (residues 350–403), an additional 35 residues from other DBP regions are also involved in the interaction. Only minor folding differences are observed between the DBP conformations in the presence or absence of actin. The r.m.s. difference of 1.86 Å obtained from superimposing all common C^{α} atoms of the actin–DBP and of the DBP (PDB code 1j78; Verboven *et al.*, 2002) structures can mainly be ascribed to a different orientation of domain I and to a different folding in some loop regions. The domain-by-domain superposition gives lower r.m.s. difference values: 1.40, 1.27 and 0.46 Å for domains I, II and III, respectively. The larger r.m.s. difference value for domain I is caused by the interaction with actin and by crystal packing differences (Fig. 3). In order to allow the interaction between solvent-exposed hydrophobic DBP residues on the C-terminal helix of domain I (amino-acids 180–188) and the

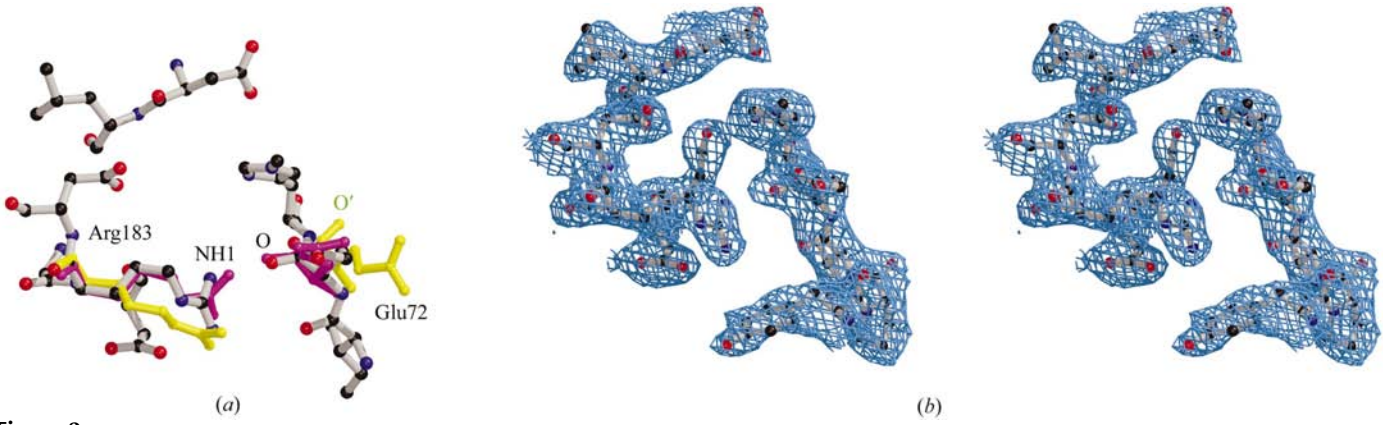

Figure 2
The hydrogen bond between Arg183 and Glu72 is unique to actin–ATP structures. (*a*) Ball-and-stick representation of residues 72 and 183 and some surrounding residues of the actin–DBP complex. Superimposed are the same two residues of the actin–ADP structure (Otterbein *et al.*, 2001), shown in pink, and the same two residues of the actin–GS1 complex (McLaughlin *et al.*, 1993), another actin–ATP complex, shown in yellow. Although the distance between Arg183 NH1 and the carbonyl O atom of Glu72 is shorter in actin–ADP (2.92 Å) than in actin–DBP (3.15 Å), in both structures the hydrogen bond can be formed. In the actin–GS1 structure the peptide bond is flipped and the carbonyl O atom (O′, shown in green) points in the opposite direction. (*b*) Stereoview of the simulated annealing $2F_o - F_c$ omit map of the same region in the same orientation as shown in (*a*).

hydrophobic cleft formed by actin subdomains 1 and 3, the C-terminal part of DBP domain I has to readjust its orientation slightly (Fig. 3). In agreement with previous biochemical observations (Van Baelen *et al.*, 1980; McLeod *et al.*, 1989), the actin–DBP structure proves that the bound actin and the observed folding differences in domain I do not hinder the binding of vitamin D_3 compounds to the vitamin D binding site of DBP (Fig. 3). All presently missing residues in the DBP structure (98–104, 318–322 and 361–364), belonging to regions that are poorly defined in the electron-density map, are located opposite the actin-binding site.

Compared with the structurally related HSA, α-fetoprotein and afamin, the third domain of DBP is largely truncated at the C-terminus. Moreover, comparison of the DBP and HSA structures revealed remarkably different orientations of the three domains in both structures (Verboven *et al.*, 2002). The shorter domain III of DBP together with its distinctive fold allows DBP to bind actin, in contrast to the other family members (Fig. 4).

The DBP residues involved in actin binding are relatively well conserved between different species in all presently known DBP sequences. Together with the highly conserved amino-acid sequence of actin throughout evolution (*e.g.* human and rabbit skeletal muscle actin are 100% identical), it explains why the actin-binding property of DBP is universally observed in vertebrates.

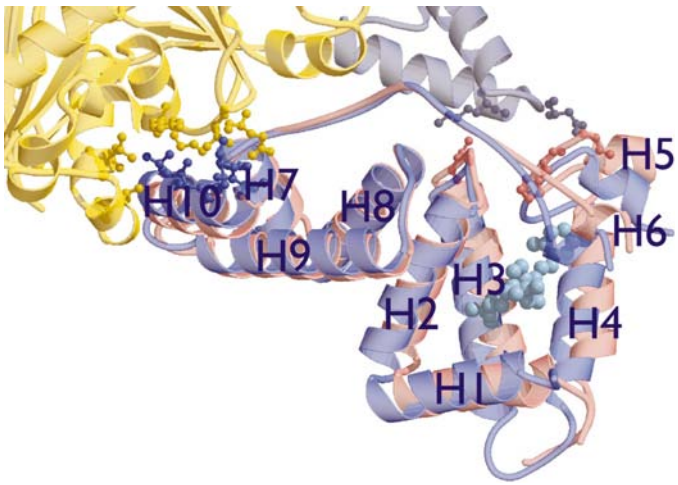

Figure 3
The superposition of the DBP domains I of actin–DBP and of the DBP–25-hydroxy vitamin D_3 (DBP–25OHD3) complex (Verboven *et al.*, 2002). Domain I of actin–DBP is shown in dark blue, actin in yellow, domain I of DBP–25OHD3 in salmon pink and a neighbouring DBP present in the DBP–25OHD3 crystal in grey. Some of the interacting residues are shown in ball-and-stick representation as well as the 25-hydroxy vitamin D_3 (pale blue). The C-terminal part of domain I (helices 7–10) of actin–DBP is shifted towards the actin to allow favourable contacts between DBP helix 10 and the cleft between actin subdomains 1 and 3. Owing to the presence of a neighbouring molecule in the DBP–25OHD3 crystal, the N-terminal part of domain I (helices 1–6; *i.e.* the vitamin D binding site) is shifted towards this neighbour to make intermolecular hydrogen bonds and hydrophobic contacts. This superposition also illustrates that the binding of a vitamin D_3 compound to DBP in the presence of actin is possible.

In comparison with α-actin, a twofold decrease of DBP-binding affinity for the non-muscle actin isoforms β-actin and γ-actin was observed (McLeod *et al.*, 1989). The actin in our actin–DBP structure originates from rabbit muscle, *i.e.* α-actin. Among the α/β or α/γ sequence differences, the residues Met/Leu176, Ala/Cys272, Tyr/Phe279 and Ile/Val287 are located in the DBP-binding site and the residues Asn/Thr297, Met/Leu299 and Thr/Ser358 are situated in its surroundings. However, *in silico* replacement of these residues in the actin–DBP structure does not result in any unfavourable contacts (Table 2) and there is no indication that the binding interface should fold differently to accommodate the replaced amino acids. Even the interaction surface between β- or γ-actin and DBP, using the modelled β- or γ-actin–DBP complex for the calculations, remains similar (3609 Å^2 compared with 3607 Å^2 for DBP–α-actin). The lower affinity of DBP for both β- and γ-actin can only be ascribed to the loss of hydrophobic interactions between DBP residues 117 and 442 and the β- or γ-actin residue 287, between DBP residue 398 and the β- or γ-actin residue 176 and between DBP residue 400 and the β- or γ-actin residue 279 (Table 2).

Although our actin–DBP structure was obtained from a crystal grown in a different space group ($P2_1$) to that of two other very recently reported actin–DBP structures [space group $P2_12_12_1$; PDB codes 1kxp (Otterbein *et al.*, 2002) and 1lot (Head *et al.*, 2002)], the structures are very similar. The C^α atoms of our actin–DBP structure and the 1lot structure superimpose with an r.m.s. difference of 0.791 Å (781 atoms superimposed), while the C^α atoms of our actin–DBP structure and the 1kxp structure superimpose with an r.m.s. difference of 0.709 Å (777 atoms superimposed). The differences between these three structures mainly reside in the loop regions and the N- and C-termini and are mainly the result of different lattice contacts. In the paper of Otterbein and coworkers, the possibility of a conformational change within the C-terminal actin residues 365–375 is proposed, since in their structure (1kxp) this region is poorly defined in the electron-density map. However, the seven extra residues 365–371 in our structure assume a similar conformation as in the other reported actin structures. The 1kxp structure and our structure have Mg^{2+}-ATP at their nucleotide-binding site, while the 1lot structure has Ca^{2+}-ATP. The presence of a different ion does not alter the conformation of ATP or the conformations of the surrounding amino acids. Only the water coordination of the ions is different: Ca^{2+} has a pentagonal bipyramidal coordination with five water molecules and two O atoms from the ATP β- and γ-phosphates, compared with the nearly octahedral coordination of Mg^{2+}, which has one fewer water molecule. In our actin–DBP structure and the 1lot structure His73 of the actin molecule is methylated, while in the 1kxp structure this is not the case. Although the peptide bond between Glu72 and His73 of actin has the same orientation in 1lot as in our structure, there is no hydrogen bond in 1lot between the main-chain carbonyl group of Glu72 and the side chain of Arg183 (see also above). In 1kxp the orientation of this peptide bond is different, making such a hydrogen bond impossible.

3.2. Binding of DBP to actin effectively interferes with actin-filament formation

Actin monomers polymerize into double-helical filaments (Fig. 5*a*) twisting around each other (Holmes *et al.*, 1990). In contrast to other types of polymerization, the actin polymerization is not linear but involves a nucleation step, with the nucleus consisting of three subunits. The resulting microfilaments are polarized: the affinity for addition of new actin monomers differs (by approximately tenfold) at the two ends. This can result, at intermediate actin-monomer concentrations, in polymerization of the filament at one end (the 'fast-growing' or 'barbed' end) and simultaneous depolymerization at the other end (the 'slow-growing' or 'pointed' end) (Wegner, 1976).

DBP binds G-actin at the side corresponding to the barbed or fast-growing end of actin in the F-actin filament. It thereby occludes actin residues 166–169 and 286–289, all of which are responsible for the longitudinal interactions between actin subunits within one F-actin strand (Holmes *et al.*, 1990). Moreover, both regions are part of a hydrophobic pocket which is postulated to be essential for the insertion of a hydrophobic plug from an actin subunit of the opposite actin strand (see also below). Although DBP does not make an immediate contact with actin residues 110–112, which are involved in interactions with an actin subunit of the opposite F-actin strand, its large volume sterically hinders the approach of the 'opposite-strand' subunit. The presence of DBP on G-actin therefore prevents the binding of two actin subunits: one that belongs in F-actin to the same strand and the other to the opposite strand (Fig. 5*a*). Hence, DBP not only blocks elongation of actin at this side, but also prohibits actin nucleation. The presence of DBP on actin seems not to hinder the interaction with other actin molecules at the pointed-end side (Fig. 5*a*). Filament growth is, however, impossible. In conditions where the molar G-actin concentration is smaller or equal to that of DBP, all G-actin subunits will be captured and blocked by DBP (Fig. 5*b*). In addition, the presence of DBP prevents the formation of the so-called lower dimer. In this actin dimer model the two actin molecules are in antiparallel orientation, a prerequisite for enabling actin polymerization (Steinmetz *et al.*, 1997).

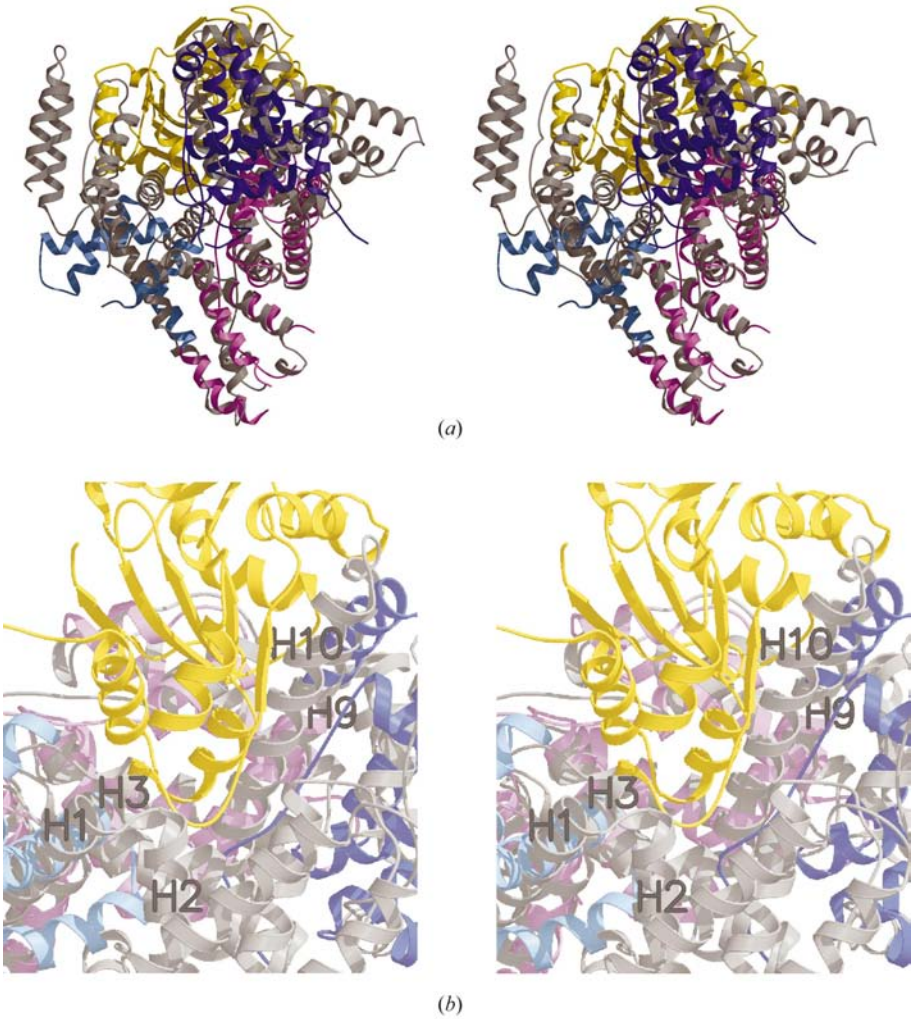

Figure 4
Superposition of the DBP from the actin–DBP structure with the HSA structure (He & Carter, 1992), illustrating that HSA cannot bind actin. (*a*) Stereoview of the overall structure of HSA (in grey) positioned on the actin–DBP structure based on the superposition of domains II of DBP and HSA. Only the actin subdomains 1 and 3 (in yellow) are shown. Domain I of DBP is shown in dark blue, domain II in pink and domain III in pale blue. The orientation of domains I–III in DBP and HSA is completely different. Consequently, the residues forming the actin-binding interface in DBP have a totally different arrangement in HSA. (*b*) Close-up view of (*a*) illustrating that owing to their different orientation, HSA helices 9 and 10 of domain I and helices 1–3 of domain III collide with parts of the actin structure.

3.3. DBP does not cap actin filaments

One of the actin subunits at the barbed end of the F-actin model (Holmes *et al.*, 1990) has its complete DBP-binding site exposed. Superposition of the actin in the actin–DBP complex with this F-actin subunit (Fig. 5*c*) seems to suggest that DBP might be able to bind to this actin with equal affinity as to G-actin and could therefore cap actin filaments. However, such activity has never been reported for DBP and even additional experiments performed to study the binding of DBP to polymeric F-actin (see §2) did not provide arguments supporting a complex of DBP with more than one actin molecule. Consequently, the F-actin model must have different folding in some of its regions in order to account for these observations.

Since the F-actin model is based on experimental data that do not permit resolution of its structure in atomic detail, some regions located at the surface of the G-actin monomer may be folded differently in the filament structure, thereby altering the DBP-binding interface. This may induce a decreased affinity between DBP and the actin subunit present in the F-actin molecule. One of the actin regions generally accepted to refold in F-actin and to be essential for the interactions between the two strands of the double-stranded F-actin is the hydrophobic plug (Holmes *et al.*, 1990; amino acids 262–274; Fig. 5*c*). It is postulated to refold as an antiparallel β-sheet inserting into the hydrophobic pocket formed by two actin subunits at the opposite F-actin strand. Moreover, since this flexible plug is located rather close to the DBP-binding interface, there is a possibility that a different conformation of the plug in the F-actin structure might hinder the binding of DBP (Fig. 5*c*). Superposition of actin from actin–DBP with the F-actin subunit having its DBP-binding site exposed illustrates that the C^{α} atoms of DBP residues 397–401 and 404 lie within a range of 8–13 Å from the C^{α} atoms of residues 270–274 of the actin plug in its 'actin-monomer' conformation. This could also serve as an explanation for the absence of growth at the pointed-end side of the actin–DBP complex (see above). The presence of DBP would prevent the refolding of the hydrophobic plug, assumed to be essential for linking both actin-filament strands.

3.4. The actin–DBP complex *versus* other actin complexes

Several structures of G-actin in complex with an actin-binding protein have already been elucidated: actin–DNase I (Kabsch *et al.*, 1990), actin–profilin (Schutt *et al.*, 1993), actin–GS1 (McLaughlin *et al.*, 1993) and actin–GS4-6 (Robinson *et al.*, 1999). The actin surface buried by the complex formation with DBP is 3600 $Å^2$, whereas the buried surfaces for the actin–DNase I, actin–GS1, actin–GS4-6 and actin–profilin

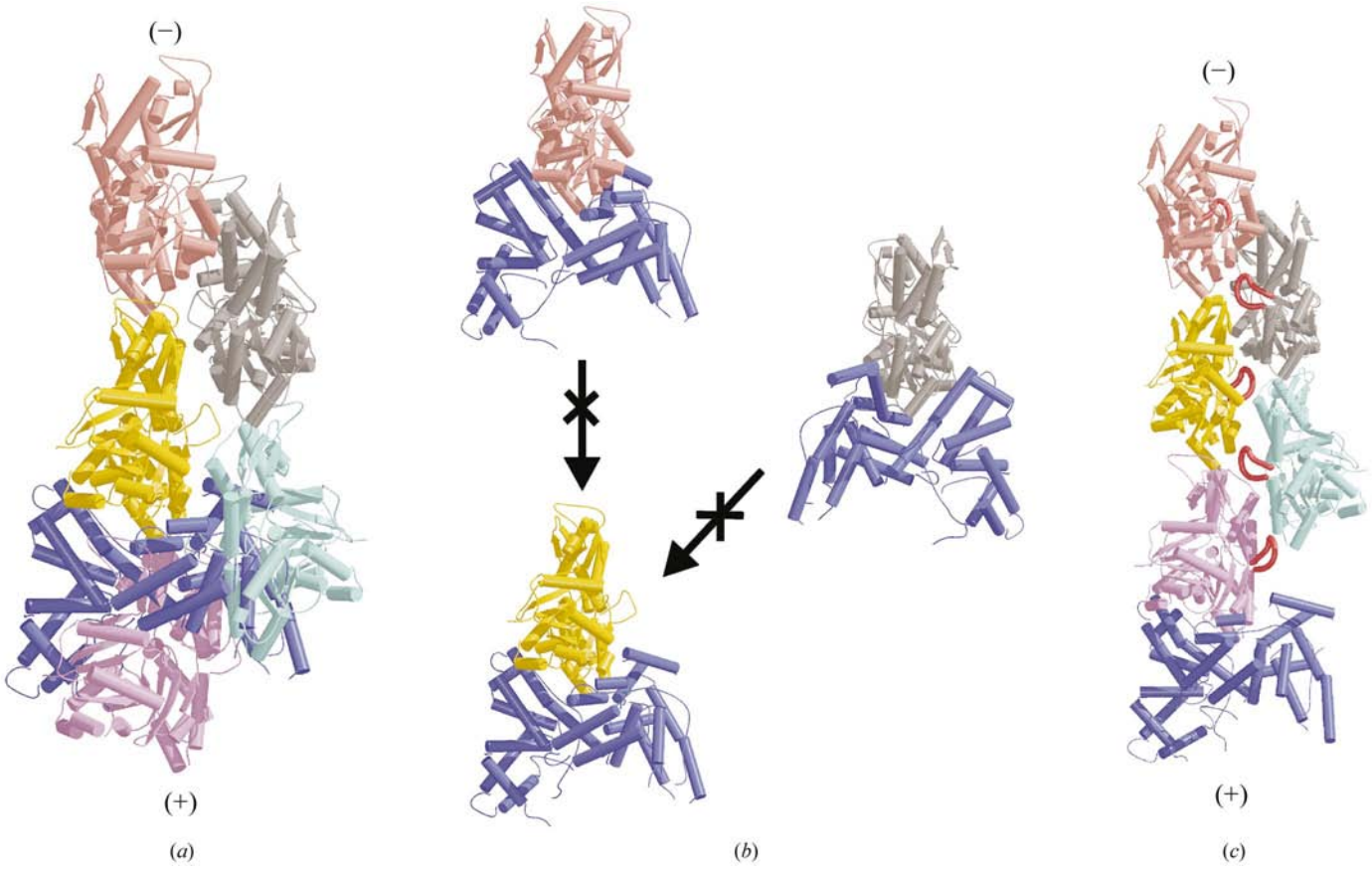

Figure 5
The binding of DBP to actin prevents actin-filament formation. (*a*) Superposition of the actin from the actin–DBP complex with the central actin subunit (yellow) of the F-actin model (Holmes *et al.*, 1990; present in PDB file 1alm; Mendelson & Morris, 1997). The five actin subunits have different colours: salmon pink, gray, yellow, pale blue and magenta. The presence of DBP (dark blue) in the actin–DBP complex prevents the binding of two subunits, which would belong in an actin filament to opposite strands: the pale blue and the magenta actin. For clarity reasons, the actin from the actin–DBP is not shown. The + and − signs indicate the fast-growing (barbed) and slow-growing (pointed) ends of F-actin, respectively. (*b*) Different actin–DBP complexes with the DBP always shown in blue and the actin in the same colours as the central actin subunit and the pointed-end actin subunits of (*a*). The presence of the bulky DBP on all actin subunits prohibits the approach of these actin subunits to another actin subunit. (*c*) The same as (*a*), illustrating that DBP can bind to this F-actin model. The actin–DBP structure is positioned here on the magenta subunit by superimposing the actins. For clarity reasons, the actin of actin–DBP is not shown. The hydrophobic plug formed by residues 262–274 is shown in red and in its conformation of the actin-monomer structures. The DBP is shown in dark blue. A refolding and a different orientation of the red hydrophobic plug may hinder the binding of DBP: the closest distance between C^{α} atoms of DBP and the hydrophobic plug in 'actin-monomer' conformation is already 8 Å.

complexes are 1800, 2100, 2100 and 2000 Å^2, respectively. Of all these complexes, DBP has the largest binding interface, indicating that the actin–DBP interaction is not merely fortuitous.

The DNase I binding site of actin, consisting of residues from subdomains 2 and 4, is located opposite the DBP-binding site (subdomains 1 and 3). This corroborates the observation that the ternary complex of DBP, DNase I and actin can be formed *in vitro* (Van Baelen *et al.*, 1980; Goldschmidt-Clermont *et al.*, 1985) (Fig. 6). The interaction surfaces of profilin, gelsolin segment 1 and gelsolin segments 4–6 are all located at the same side of actin as the DBP-binding site and are all partially overlapping (Fig. 6). This structural comparison also demonstrates how DBP bound to actin obstructs its further interaction with profilin, as previously observed (Goldschmidt-Clermont *et al.*, 1986).

Gelsolin, consisting of six segments of 120–130 amino acids each (S1–S6), has been reported to nucleate growth through the binding of two actin monomers in an appropriate orientation. DBP can prevent reformation of actin filaments by reducing the effective G-actin concentration. The observation that DBP is capable of displacing one actin from the ternary gelsolin–actin (1:2) complex may also play a role in inhibiting the nucleation (Janmey *et al.*, 1986). However, current understanding of the structural organization of the gelsolin–actin (1:2) complex does not permit explanation of how DBP can remove one actin from it. In the proposed model of this ternary complex (Robinson *et al.*, 1999), the DBP-binding interface is blocked in both actins either by segment 1 or by segment 4 of gelsolin. However, another study, involving cross-linking experiments with different gelsolin constructs, indicated that a ternary complex with the two actins in appropriate orientation for filament growth (Hesterkamp *et al.*, 1993) is formed only with gelsolin segments 2–6, whereas with the whole gelsolin the actin monomers are in an antiparallel orientation as in the lower actin dimer.

Figure 6
Superposition of actin-complex structures: actin–DNase I (Kabsch *et al.*, 1990), actin–profilin (Schutt *et al.*, 1993), actin–GS1 (McLaughlin *et al.*, 1993), actin–GS4-6 (Robinson *et al.*, 1999) and actin–DBP. All these complexes are superimposed based on the superposition of their actins. For clarity reasons, only the actin of actin–DNase I is shown (in yellow). DNase I is shown in grey, profilin in salmon pink, gelsolin segment 1 in pale blue, gelsolin segment 4–6 in magenta and DBP in dark blue.

It is noteworthy that DBP, gelsolin segment 1 and gelsolin segment 4–6 have a hydrophobic helix that interacts with the hydrophobic patch in the cleft between subdomains 1 and 3 of actin. It can be postulated that other proteins binding actin at the barbed-end side and having an appropriate helix with solvent-accessible hydrophobic residues will bind to actin in such an orientation that this helix is also located in the cleft between subdomains 1 and 3 (Fig. 6). This may be the case for the N-terminal helix of the actin-sequestering β-thymosins. Such an orientation of this helix would explain the crosslinks between thymosin β_4 and actin: Lys3–Glu167 and Lys18–Asp1 (Safer *et al.*, 1997). Moreover, it has previously been suggested that thymosin β_4 interacts with actin through a patch of hydrophobic residues located on the N-terminal helix (Van Troys *et al.*, 1996). This hypothesis also supports the previously suggested idea that the α3 helix of cofilin (Fedorov *et al.*, 1997), an actin-severing protein, could interact in a similar manner with actin as its corresponding α-helix in gelsolin.

3.5. Implications for the extracellular actin-scavenger system

The observed perfect fit between actin and DBP, as illustrated here, provides the structural basis for the important role of DBP in the extracellular actin-scavenger system. Furthermore, although DBP and gelsolin are both present in large concentrations (micromolar) in blood, their capacity to scavenge actin may still be overwhelmed during massive cell injury. Indeed, the saturation of the actin-scavenger system leads to formation of thrombi and microangiopathy (Haddad *et al.*, 1990; Erukhimov *et al.*, 2000), and excessive amounts of actin in the circulation may lead to a condition resembling 'multiple organ dysfunction syndrome'. The latter syndrome was found to be associated with reduced serum DBP levels (Schiødt *et al.*, 1997; Dahl *et al.*, 1998). Moreover, DBP serum concentrations are reduced in some patients with hepatic failure (Schiødt *et al.*, 1995, 1997). The DBP concentrations not only have some value in predicting survival from hepatic failure (Lee *et al.*, 1995; Schiødt *et al.*, 1996), but may also identify patients at high-risk after multiple trauma (Dahl *et al.*, 1999). Consequently, the actin–DBP structure, revealing the

DBP residues essential for the interaction with actin and for actin sequestering, is of major importance for the development of a drug that could be applied in the above-mentioned pathological conditions.

Despite intensive analysis, no DBP-deficient individual has been identified, leading to the suggestion that certain functions of DBP might be essential for survival. However, viable DBP-knockout mice could be generated (Safadi *et al.*, 1999). These mice were only used for analysis of the role of DBP in vitamin D metabolism and action. Although DBP-knockout mice are viable under normal laboratory conditions, it might well be that the role of DBP in the actin-scavenger system is essential for survival in the case of severe tissue damage. This would be in line with our striking structural observations and the perfect conservation of DBP–actin interaction during the evolution of vertebrates.

In the actin–GS1 (McLaughlin *et al.*, 1993), actin–GS4-6 (Robinson *et al.*, 1999), actin–profilin (Schutt *et al.*, 1993) and actin–DBP complexes and in actin covalently linked to tetramethylrhodamine-5-maleimide (actin–TMR; Otterbein *et al.*, 2001), actin-filament formation is blocked at the barbed-end side. The structures of all these complexes illustrate that all these actin ligands block the cleft between subdomains 1 and 3. Even a small molecule such as TMR is able to prevent filament formation. Intracellular sequestering proteins such as thymosin β_4 (5 kDa) and profilin (15 kDa) are rather small compared with their extracellular counterpart DBP (51 kDa). These remarkable differences in size of the actin-interaction surfaces between the extracellular and intracellular sequestering proteins might be related to the fact that in the intracellular compartment an equilibrium between G-actin and F-actin has to be maintained. In extracellular space F-actin formation has to be prevented at any cost. Therefore, DBP, a better actin-sequestering protein, is present in high concentrations in the extracellular compartment.

We thank the staff of the EMBL beamlines at the DORIS storage ring, DESY, Hamburg for their support during the data collection and the European Community for their support for travel to the EMBL Hamburg Outstation through their Access to Research Infrastructure Action of the Improving Human Potential Programme. This work was in part supported by the K. U. Leuven Research Fund and by the 'Fonds voor Wetenschappelijk Onderzoek (FWO) – Vlaanderen'.

References

Bogaerts, I., Verboven, C., Rabijns, A., Waelkens, E., Van Baelen, H. & De Ranter, C. (2001). *Acta Cryst.* D**57**, 740–742.
Brünger, A. T., Adams, P. D., Clore, G. M., DeLano, W. L., Gros, P., Grosse-Kunstleve, R. W., Jiang, J. S., Kuszewski, J., Nilges, M., Pannu, N. S., Read, R. J., Rice, L. M., Simonson, T. & Warren, G. L. (1998). *Acta Cryst.* D**54**, 905–921.
Burtnick, L. D., Koepf, E. K., Grimes, J., Jones, E. Y., Stuart, D. I., McLaughlin, P. J. & Robinson, R. C. (1997). *Cell*, **90**, 661–670.
Cooke, N. E. & Haddad, J. G. (1989). *Endocr. Rev.* **10**, 294–307.
Dahl, B., Schiødt, F. V., Kiær, T., Ott, P., Bondesen, S. & Tygstrup, N. (1998). *Crit. Care Med.* **26**, 285–289.
Dahl, B., Schiødt, F. V., Nielsen, M., Kiær, T., Williams, J. G. & Ott, P. (1999). *Injury*, **30**, 275–281.
Dueland, S., Nenseter, M. S. & Drevon, C. A. (1991). *Biochem. J.* **274**, 237–241.
Erukhimov, J. A., Tang, Z.-L., Johnson, B. A., Donahoe, M. P., Razzack, J. A., Gibson, K. F., Lee, W. L., Wasseloos, K. J., Watkins, S. A. & Pitt, B. R. (2000). *Am. J. Respir. Crit. Care Med.* **162**, 288–294.
Esnouf, R. M. (1997). *J. Mol. Graph.* **15**, 132–134.
Fedorov, A. A., Lappalainen, P., Fedorov, E. V., Drubin, D. G. & Almo, S. C. (1997). *Nature Struct. Biol.* **4**, 366–369.
Goldschmidt-Clermont, P. J., Galbraith, R. M., Emerson, D. L., Marsot, F., Nel, A. E. & Arnaud, P. (1985). *Biochem. J.* **228**, 471–477.
Goldschmidt-Clermont, P. J., Van Alstyne, E. L., Day, J. R., Emerson, D. L., Nel, A. E., Lazarchick, J. & Galbraith, R. M. (1986). *Biochemistry*, **25**, 6467–6472.
Goldschmidt-Clermont, P. J., Van Baelen, H., Bouillon, R., Shook, T. E., Williams, M. H., Nel, A. E. & Galbraith, R. M. (1988). *J. Clin. Invest.* **81**, 1519–1527.
Haddad, J. G., Harper, K. D., Guoth, M., Pietra, G. G. & Sanger, J. W. (1990). *Proc. Natl Acad. Sci. USA*, **87**, 1381–1385.
Haddad, J. G., Hu, Y. Z., Kowalski, M. A., Laramore, C., Ray, K., Robzyk, P. & Cooke, N. (1992). *Biochemistry*, **31**, 7174–7181.
He, X. M. & Carter, D. C. (1992). *Nature (London)*, **358**, 209–215.
Head, J. F., Swamy, N. & Ray, R. (2002). *Biochemistry*, **41**, 9015–9020.
Herrmannsdoerfer, A. J., Heeb, G. T., Feustel, P. J., Estes, J. E., Keenan, C. J., Minnaer, F. L., Selden, L., Giunta, C., Flor, J. R. & Blumenstock, F. A. (1993). *Am. J. Physiol.* **265**, G1071–G1081.
Hesterkamp, T., Weeds, A. G. & Mannherz, H. G. (1993). *Eur. J. Biochem.* **218**, 507–513.
Holmes, K. C., Popp, D., Gebhard, W. & Kabsch, W. (1990). *Nature (London)*, **347**, 44–49.
Houmeida, A., Hanin, V., Constans, J., Benyamin, Y. & Roustan, C. (1992). *Eur. J. Biochem.* **203**, 499–503.
Janmey, P. A., Stossel, T. P. & Lind, S. E. (1986). *Biochem. Biophys. Res. Commun.* **136**, 72–79.
Jones, T. A., Zou, J.-Y., Cowan, S. W. & Kjeldgaard, M. (1991). *Acta Cryst.* A**47**, 110–119.
Kabsch, W., Mannherz, H. G., Suck, D., Pai, E. F. & Holmes, K. C. (1990). *Nature (London)*, **347**, 37–44.
Kleywegt, G. J., Zou, J.-Y., Kjeldgaard, M. & Jones, T. A. (2001). *International Tables for Crystallography*, Vol. F, edited by M. G. Rossmann & E. Arnold, pp. 353–367. Dordrecht: Kluwer Academic Publishers.
Kraulis, P. J. (1991). *J. Appl. Cryst.* **24**, 946–950.
Laemmli, U. K. (1970). *Nature (London)*, **227**, 680–685.
Lee, W. M. & Galbraith, R. M. (1992). *N. Engl. J. Med.* **326**, 1335–1341.
Lee, W. M., Galbraith, R. M., Watt, G. H., Hughes, R. D., McIntire, D. D., Hoffman, B. J. & Williams, R. (1995). *Hepatology*, **21**, 101–105.
Lind, S. E., Smith, D. B., Janmey, P. A. & Stossel, T. P. (1986). *J. Clin. Invest.* **78**, 736–742.
McLaughlin, P. J., Gooch, J. T., Mannherz, H. G. & Weeds, A. G. (1993). *Nature (London)*, **364**, 685–692.
McLeod, J. F., Kowalski, M. A. & Haddad, J. G. (1989). *J. Biol. Chem.* **264**, 1260–1267.
Mendelson, R. & Morris, E. P. (1997). *Proc. Natl Acad. Sci. USA*, **94**, 8533–8538.
Merritt, E. A. & Murphy, M. E. P. (1994). *Acta Cryst.* D**50**, 869–873.
Otterbein, L. R., Cosio, C., Graceffa, P. & Dominguez, R. (2002). *Proc. Natl Acad. Sci. USA*, **99**, 8003–8008.
Otterbein, L. R., Graceffa, P. & Dominguez, R. (2001). *Science*, **293**, 708–711.
Otwinowski, Z. & Minor, W. (1997). *Methods Enzymol.* **276**, 307–326.

Robinson, R. C., Mejillano, M., Le, V. P., Burtnick, L. D., Yin, H. L. & Choe, S. (1999). *Science*, **286**, 1939–1942.
Safadi, F. F., Thornton, P., Magiera, H., Hollis, B. W., Gentile, M., Haddad, J. G., Liebhaber, S. A. & Cooke, N. E. (1999). *J. Clin. Invest.* **103**, 239–251.
Safer, D., Sosnick, T. R. & Elzinga, M. (1997). *Biochemistry*, **36**, 5806–5816.
Schiødt, F. V., Bondesen, S., Petersen, I., Dalhoff, K., Ott, P. & Tygstrup, N. (1996). *Hepatology*, **23**, 713–718.
Schiødt, F. V., Bondesen, S. & Tygstrup, N. (1995). *Eur. J. Gastroenterol. Hepatol.* **7**, 635–640.
Schiødt, F. V., Ott, P., Bondesen, S. & Tygstrup, N. (1997). *Crit. Care Med.* **25**, 1366–1370.
Schutt, C. E., Myslik, J. C., Rozycki, M. D., Goonesekere, N. C. W. & Lindberg, U. (1993). *Nature (London)*, **365**, 810–816.
Steinmetz, M. O., Stoffler, D., Hoenger, A., Bremer, A. & Aebi, U. (1997). *J. Struct. Biol.* **119**, 295–320.
Van Baelen, H., Bouillon, R. & De Moor, P. (1980). *J. Biol. Chem.* **255**, 2270–2272.
Van Troys, M., Dewitte, D., Goethals, M., Carlier, M. F., Vandekerckhove, J. & Ampe, C. (1996). *EMBO J.* **15**, 201–210.
Vasconcellos, C. A. & Lind, S. E. (1993). *Blood*, **82**, 3648–3657.
Verboven, C. C., De Bondt, H. L., De Ranter, C. J., Bouillon R. & Van Baelen, H. (1995). *J. Steroid Biochem. Mol. Biol.* **54**, 11–14.
Verboven, C., Rabijns, A., De Maeyer, M., Van Baelen, H., Bouillon, R. & De Ranter, C. (2002). *Nature Struct. Biol.* **9**, 131–136.
Wegner, A. (1976). *J. Mol. Biol.* **108**, 139–150.
White, P. & Cooke, N. (2000). *Trends Endocrinol. Metab.* **11**, 320–327.